



Exhumation and carbonation of the Atlantis Bank core complex constrained by *in situ* U-Pb dating and Δ_{47} thermometry of calcite veins, SW Indian Ridge

Mark A. Kendrick^{a,*}, Oliver Plümper^b, Jian-Xin Zhao^a, Yuexing Feng^a, William F. Defliese^a, Inigo A. Müller^b, Martin Ziegler^b

^a School of Earth and Environmental Sciences, The University of Queensland, St Lucia, 4072 Queensland, Australia

^b Department of Earth Sciences, Utrecht University, 3584 CD Utrecht, The Netherlands

ARTICLE INFO

Article history:

Received 8 August 2021

Received in revised form 15 February 2022

Accepted 24 February 2022

Available online 24 March 2022

Editor: L. Coogan

Keywords:

calcium carbonate vein

U-Pb dating

clumped isotopes

oceanic core complex

ABSTRACT

The Atlantis Bank is a representative example of an oceanic core complex formed on a slow-spreading ridge. It is dominated by olivine gabbros emplaced at ~ 12 Ma and exhumed from original depths of more than ~ 2500 metres below seafloor (mbsf). In order to investigate the timing of exhumation and low-temperature alteration we investigated twenty-two calcite veins in samples of core recovered from the 809-mbsf Hole U1473A drilled during Expedition 360 of the International Ocean Discovery Program. The calcite veins yielded laser ablation U-Pb and bulk U-Th ages ranging from 10.4 ± 0.3 Ma to 273 ± 5 Ka. They have an average Δ_{47} formation temperature of $21 \pm 4^\circ\text{C}$ and $^{87}\text{Sr}/^{86}\text{Sr}$ and rare earth element signatures typical of low-temperature veins dominated by seawater. These data preclude previous cooling models that invoked a 250°C heat pulse related to sill emplacement at ~ 9.4 Ma. Instead, the combined Δ_{47} and U-Pb age data indicate a simple cooling path in which the gabbros were exhumed close to the seafloor and cooled to a mean of $21 \pm 4^\circ\text{C}$ by 10.4 ± 0.3 Ma. The timing of the earliest low-temperature veins 1.6 ± 0.7 Myr after accretion is broadly similar to that reported for other oceanic core complexes. However, the 12 Ma age of the Atlantis Bank means it has recorded a longer carbonation history. The vein ages indicate $\sim 83\%$ of vein growth occurred during a period of 3.1 ± 0.9 Myr between ~ 10.4 and ~ 7.3 Ma. The Atlantis Bank gabbros are estimated to have a bulk concentration of 0.15 ± 0.04 wt% CO_2 . Therefore if carbonation and veining occurred proportionally to one another, the initial carbonation rate was $\sim 400 \pm 200$ $\mu\text{g/g CO}_2$ per Myr. A single vein with an age of 5.8 ± 0.4 Ma formed between 7.3 and 1 Ma suggesting a virtual hiatus in carbonation. However, resumed vein growth after 0.27–1 Ma is recorded by three samples. The uncertainty in these very young U-Pb ages is substantial, meaning the carbonation rate is only loosely constrained as similar to, or lower than, the initial rate of ~ 400 $\mu\text{g/g CO}_2$ per Myr. These data demonstrate that recent carbonation of 12 Ma old ocean crust is significant and probably ongoing. Given that ocean core complexes form on crustal-scale detachments that provide high permeability pathways, and they are bathymetric highs where reactive lithologies can be exposed on the seafloor, oceanic core complexes like the Atlantis Bank could be sites of long-lived alteration on the seafloor.

© 2022 The Author(s). Published by Elsevier B.V. This is an open access article under the CC BY-NC-ND license (<http://creativecommons.org/licenses/by-nc-nd/4.0/>).

1. Introduction

Oceanic core complexes, where low angle detachment faults expose basement gabbros and reactive peridotite lithologies on the seafloor, constitute an important mode of extension on slow-

spreading ridges (e.g. Dick et al., 2000; Baines et al., 2008). This study uses recently developed *in situ* calcite U-Pb dating and clumped isotope thermometry to investigate the timing and temperature of carbonate vein growth in basement gabbros exposed on the Atlantis Bank, which is a representative example of an oceanic core complex on the Southwest Indian Ridge (Fig. 1; Dick et al., 2019).

Carbonate clumped isotope thermometry allows the temperature of carbonate vein formation and the $\delta^{18}\text{O}_{\text{fluid}}$ of the alteration

* Corresponding author.

E-mail address: m.kendrick@uq.edu.au (M.A. Kendrick).

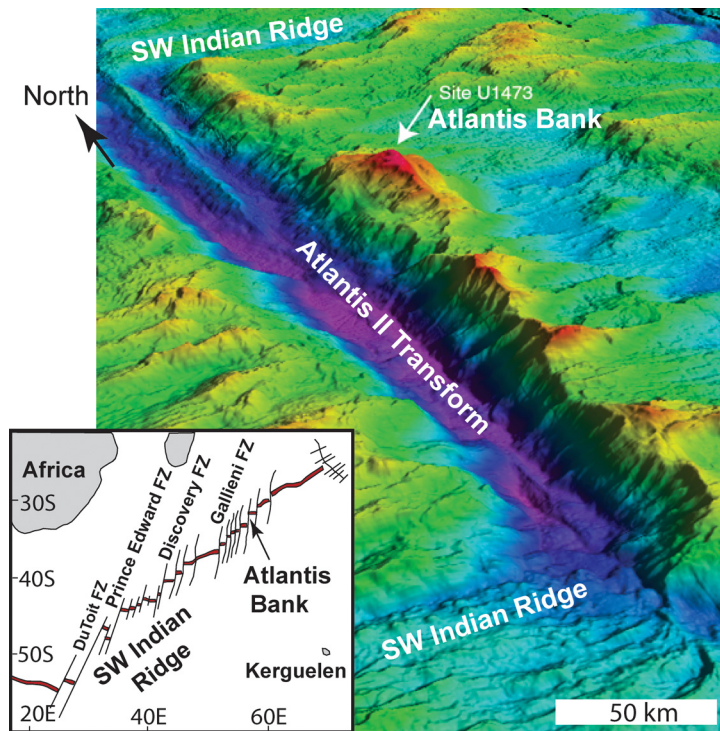


Fig. 1. Bathymetry of the Atlantis II Transform (water depth ~ 6000 -m) showing the position of the Atlantis Bank ~ 100 km south of the SW Indian Ridge (water depth ~ 700 -m; MacLeod et al., 2017) and inset map showing the position on the Southwest Indian Ridge. Scale bar is approximate. (All figures are in colour in the web version of this article.)

fluid to be determined independently of each other, based on the isotopic composition and ordering of ^{18}O and ^{13}C in the carbonate group (Eiler, 2007). The isotopic ordering is reported as Δ_{47} , which defines the deviation of the abundance of clumped CO_2 isotopologues with mass 47 from their theoretical abundance based on a stochastic distribution. Combining the temperature of vein growth with the formation age obtained by *in situ* U-Pb dating means that calcite veins can provide thermochronological constraints on basement uplift and exhumation that are complementary to traditional high temperature (zircon U-Pb, mica Ar-Ar) and low temperature (U/Th-He and fission track) chronometers (cf. John et al., 2004; Schwartz et al., 2009; Rioux et al., 2016).

The timing of the earliest carbonate vein growth provides information about when brittle faulting related to basement exhumation on the Atlantis Bank was initiated and the distribution of vein ages provides information about the duration and continuity of low temperature alteration. This is important because the timing of fault movements on oceanic core complexes relative to crustal accretion (e.g. gabbro emplacement) and the uplift and exhumation history are incompletely understood (cf. John et al., 2004; Schwartz et al., 2009).

Furthermore, low-temperature carbonate alteration, which is commonly associated with clay minerals and Fe-oxyhydroxides may exert a significant influence on the composition of seawater and the inventory of volatiles and fluid mobile elements in oceanic crust that is subducted into the mantle (Staudacher and Allègre, 1988; Alt and Teagle, 1999; Staudigel, 2014; Kendrick et al., 2020b). Despite its importance, the duration of active seafloor alteration and carbonation is still poorly constrained (Bach et al., 2001; Staudigel, 2014; Coogan et al., 2016; Laureijs et al., 2021). This is because a small number of studies have investigated alteration chronology and earlier methods including Sr isotope model ages for calcite vein growth (Staudigel and Hart, 1985) and Rb-Sr dating of celadonite (Booij et al., 1995) were limited by relatively low precision and the need to group multiple samples together to define isochrons.

Laser ablation methods for U-Pb dating of calcite and Rb-Sr dating of celadonite have recently become available and provide the potential to more easily investigate multi-stage alteration histories (e.g. Coogan et al., 2016; Laureijs et al., 2021). Laser ablation enables rapid microsampling of carbonate domains with variable U/Pb ratios at microscopic scales. The variability of U/Pb in carbonate means that spot analyses for individual veins can be plotted in Tera-Wasserberg concordia diagrams to define isochrons with lower concordia intercepts that yield meaningful U-Pb ages (e.g. Coogan et al., 2016; Roberts et al., 2017; MacDonald et al., 2019). Furthermore, sector-field inductively coupled plasma mass spectrometry (ICPMS) has sufficiently high sensitivity that U and Pb isotopes can be measured in spot sizes of less than $100\ \mu\text{m}$ even when U is present at sub- $\mu\text{g/g}$ levels in Quaternary age samples. The method therefore provides an ideal tool for testing if alteration and carbonation of the Atlantis Bank has occurred continuously throughout its 12 Ma history or in a limited number of discrete events.

The combination of age information and clumped isotope analysis, which provides $\delta^{18}\text{O}_{\text{fluid}}$ and $\delta^{13}\text{C}$, with other geochemical proxies including Sr isotopes and trace elements also provides new insights into the evolution of a modern fluid alteration system in an oceanic core complex. This is important for understanding how carbonate veins can be used as archives for palaeo-seawater composition (Coogan et al., 2010) and the nature of low-temperature alteration fluids advecting through the crust (Staudigel and Hart, 1985; Alt and Teagle, 1999; Bach et al., 2001; Kendrick, 2019).

1.1. The Atlantis Bank core complex

The Atlantis Bank is a bathymetric high adjacent to the Atlantis II Transform, which offsets the slow spreading Southwest Indian Ridge (Fig. 1). The summit of the Atlantis Bank has a water depth of only ~ 700 m and has been investigated in detail utilising manned and remote underwater vehicles, dredging, seabed drilling and two deep basement drill holes (Dick et al., 2000, 2019).

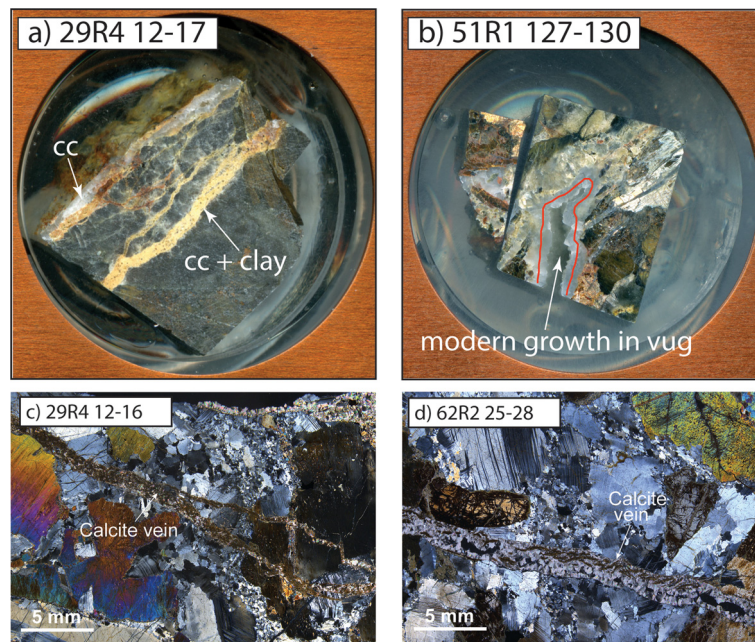


Fig. 2. Representative examples of the calcite veins featured in this study. Polished blocks (2.5 cm diameter) of a) 29R4 12-17 and b) 51R1 127-130. Photomicrographs of calcite veins crosscutting gabbro in c) 29R4 12-16 and d) 62R2 25-28. Calcite within the veins varies in grain-size but typically exhibits blocky or syntaxial growth patterns. Note that carbonate in the vug in 51R1 127-130 gave a younger age than carbonate elsewhere in the sample.

Together with surface mapping, the 1508-mbsf Hole 735B drilled by Legs 118 (1987) and 176 (1997) of the Ocean Drilling Program (Dick et al., 2000), and the 809-mbsf Hole U1473A drilled by Expedition 360 (2015/16) of the International Ocean Discovery Program (Dick et al., 2019), provide an unprecedented section through crust formed on a slow-spreading ridge.

The Bank is dominated by olivine gabbro, with lesser amounts of primitive troctolite in Hole 735B and evolved oxide gabbros (>5% Fe-oxide) and felsic veins in Holes 735B and U1473A (Dick et al., 2000, 2019; MacLeod et al., 2017). The oxide gabbros are interpreted as late-stage melts. The felsic veins account for ~2 vol.% of the recovered core and transect the earlier gabbros (Dick et al., 2000, 2019). Zircons, sphenes and apatites have been separated from the oxide gabbros and felsic veins (John et al., 2004; Schwartz et al., 2009). The Ti-in-zircon thermometer indicates zircon crystallisation at 750–950 °C (Rioux et al., 2016). High precision isotope dilution TIMS dating of zircons indicate Hole 735B gabbros were emplaced over a period of ~200–300 ka between 12.18 ± 0.07 Ma and 11.90 ± 0.01 Ma (Rioux et al., 2016).

The Atlantis Bank gabbros record a prolonged alteration history extending from upper amphibolite facies when initial hydration occurred in response to late-stage magmatic fluids and the influx of seawater (Dick et al., 2000, 2019; Nozaka et al., 2019), to late-stage carbonation (Bach et al., 2001; Alt and Bach, 2006; Kendrick, 2019; Kendrick et al., 2020a). Fluid inclusions in amphibolite facies minerals record pressures consistent with the emplacement of Hole 735B (0–1500 mbsf) gabbros at depths of ~1600–3100 mbsf in a >4 km thick crust (Vanko and Stakes, 1991). Following initial alteration, the Atlantis Bank was then unroofed and exhumed to sea-level before subsiding to its current water depth of ~700 m (Fig. 1; Dick et al., 2000, 2019; MacLeod et al., 2017).

Carbonate veins associated with Fe-oxyhydroxide and clay minerals have a relatively high abundance between ~500 and 800 mbsf in Hole 735B (Bach et al., 2001) and between ~200 and 600 mbsf in Hole U1473A (MacLeod et al., 2017; Dick et al., 2019; Kendrick, 2019). The carbonate has a high iodine concentration of 5–26 ppm that demonstrates formation from oxidised fluids

that were enriched in iodate relative to seawater (Kendrick et al., 2020a). Previous oxygen isotope thermometry suggests carbonate veins formed at temperatures of ~10 °C in Hole 735B (Alt and Bach, 2006).

A range of geochronometers and thermochronometers have been applied to Atlantis Bank lithologies (John et al., 2004; Schwartz et al., 2009). In addition to the ~12 Ma zircon U-Pb emplacement ages (Rioux et al., 2016), the uplift and exhumation history has been partially constrained via biotite Ar-Ar plateau ages averaging ~11.4 Ma (John et al., 2004), and fission-track and U-Th-He ages of zircon, sphene and apatite that extend down to 7.2 Ma (John et al., 2004; Schwartz et al., 2009). These data have been interpreted as indicating rapid cooling to <200 °C by ~11 Ma followed by a thermal pulse related to the emplacement of a sill in an off-axis setting re-heating the gabbros at ~9.4 Ma, ~2.6 Myr after accretion (Schwartz et al., 2009). This hypothesis has significant implications for how oceanic crust is formed, the timing of movement on the Atlantis Bank detachment fault, and the sources of heat driving late-stage alteration.

2. Samples and methodology

Representative carbonate veins were selected from Hole U1473A drill core during Expedition 360. Most of the veins sampled contain coarse sparry calcite that are typically 1–3 mm in thickness (Fig. 2). Most have blocky textures and/or vugs demonstrating growth from the wallrock into voids. The calcite veins transect all other alteration types but are closely associated with red-brown coloured Fe-oxyhydroxide (limonite), which replaces olivine and orthopyroxene, and smectite, which is present along the margins of some calcite veins (Fig. 2b and c; Kendrick et al., 2020a). Examination of the veins by Raman spectroscopy confirms the majority are low-Mg calcite (Fig. S1, Electronic supplement), and inspection of doubly polished fluid inclusion wafers prepared from three large veins revealed an absence of fluid inclusions (Kendrick et al., 2020a).

2.1. U-Pb dating and trace elements

Twenty-one veins were mounted in epoxy and polished to a one micron finish for laser ablation (Fig. 2) in the Radiogenic Isotope Facility (RIF) at the University of Queensland. Trace element analysis and U/Pb screening were accomplished using an Australian Scientific Instruments (ASI) RESOLUTION 193 nm excimer ArF laser coupled to a Thermo Fisher iCAP RQ inductively coupled plasma mass spectrometer (ICP-MS). Trace element analyses were typically undertaken on 8–10 spots per sample and U/Pb screening on 80–100 spots (100 μm diameter, 10 Hz, 3 J cm^{-2}). The measurement cycle for trace elements included a 20 s background, 25 s ablation and 10 s washout time. However, a shortened cycle utilising 3 second ablations was used for U/Pb screening, where the only purpose was to identify domains with high U/Pb ratio. Following screening, domains with high U/Pb were targeted for U/Pb dating. The calcite-clay vein in sample 29R2 12–17 (Fig. 2a) was successfully dated using the iCAP RQ mass spectrometer. However, the laser ablation system was coupled to the high sensitivity Nu Plasma II multi-collector ICP-MS in order to satisfactorily date most of the calcite samples. ^{238}U , ^{206}Pb , ^{207}Pb , ^{208}Pb were measured by ion counting with a 20 second background, 20 second ablation and 20 second washout time (see Electronic Supplement for details).

The time-resolved data were reduced using the Iolite software v. 3.71 (Paton et al., 2011). NIST614 was used as the primary standard for trace element and U/Pb isotope analysis. NIST 612 was analysed as an unknown and gave trace element concentrations within 1–4% of their reference values (Electronic Supplement). The U/Pb age data were plotted in Tera-Wasserburg Concordia diagrams using the Isoplot 3.76 program (Ludwig, 2012) and renormalised to laboratory calcite U-Pb reference materials (AHX-1a or AHX-1b). The uncertainties in the ages determined by Model 1 regressions include the Student's-t multiplier (Ludwig, 2012). Additional reference materials (WC-1 and PTKD-2) were analysed as unknowns and returned ages within uncertainty of the independently calibrated reference values of 153.7 ± 1.7 Ma for PTKD-2 and 254.4 ± 6.4 Ma for WC-1 (Roberts et al., 2017; see Electronic supplement for additional references and details; Figs. S2 and S3).

2.2. Clumped isotopes

Twenty one vein samples were prepared as powders and analysed for clumped isotopes at the University of Utrecht using a Kiel III carbonate device coupled to a MAT253 isotope ratio mass spectrometer or a Kiel IV carbonate device coupled to a 253 Plus isotope ratio mass spectrometer (Thermo Fisher Scientific) (Meckler et al., 2014). Samples (150 μg for MAT253; 70–90 μg for 253 Plus) were analysed as multiple repeats ($n = 15$ –21 for most samples) and bracketed by standards (ETH-1, -2, -3, -4). In total 293 sample replicates were analyzed. The samples were reacted with 102% phosphoric acid at 70 °C for 360 s and the evolved gas was purified in multiple steps. First, the gas was transferred to a cryogenic liquid nitrogen (LN_2) trap at -196°C , which traps CO_2 and removes non-condensable gases. The impure CO_2 was then transferred (400 s) to a second cold trap through a Porapak-Q trap (mesh size 50–80 μm) at -40°C to remove organic contaminants, such as halo-/hydrocarbons and reduced sulfur compounds. The purified CO_2 gas was admitted into the mass spectrometer at 30 °C and measured for its m/z 44 to 49 intensities.

Raw intensities were corrected for a negative pressure baseline using peak shape scans performed before each run (Meckler et al., 2014) and corrected to the Intercarb-Carbon Dioxide Equilibrium Scale (I-CDES). This was achieved by creating an empirical transfer function (ETF) using recommended values of the ETH standards (ETH-1, -2, -3 and -4) (Bernasconi et al., 2021). The ETF

for each sample aliquot was calculated from ~ 100 standard measurements undertaken before and after each aliquot over a period encompassing ~ 3 weeks. Δ_{47} , $\delta^{18}\text{O}$, $\delta^{13}\text{C}$ were calculated using the latest IUPAC values for isotopic abundances in VSMOW and VPDB (Daëron et al., 2016). The oxygen isotope composition of the carbonate has been corrected for acid digestion at 70 °C using a fractionation factor of 1.00871 (Kim et al., 2007). Repeat analyses of two check standards IAEA-C2 and MERCK have mean I-CDES Δ_{47} values (± 1 s.d.) of $0.633 \pm 0.038\text{‰}$ ($n = 111$) and $0.506 \pm 0.043\text{‰}$ ($n = 82$) that agree well with results presented in the Intercarb study (Bernasconi et al., 2021).

Temperatures were obtained from the Δ_{47} values using calibration of Anderson et al. (2021) which is consistent with the I-CDES reference frame. The $\delta^{18}\text{O}_{\text{fluid}}$ of the fluid was calculated relative to VSMOW based on the temperature-dependent oxygen isotope fractionation between calcite and water calibrated with slow-grown natural calcite (Daëron et al., 2019), using the measured clumped isotope temperature.

2.3. Sr isotope and U-Th age analysis

Calcite extracted from the central part of twelve veins was prepared as a powder. Portions of each sample (~ 15 –35 mg) were digested in dilute double-distilled nitric acid. The solutions were centrifuged to separate acid insolubles and the supernatant passed through Sr-Spec columns to separate Sr. The Sr isotope compositions were measured using a Nu Plasma II multi-collector ICP-MS at the University of Queensland. The SRM-987 reference material was measured as a drift monitor after every five samples. Sr isotope data for SRM-987 and samples were corrected for mass fractionation by normalising to $^{86}\text{Sr}/^{88}\text{Sr} = 0.1194$. The fractionation-corrected $^{87}\text{Sr}/^{86}\text{Sr}$ ratios were then normalised to NIST-987 $^{87}\text{Sr}/^{86}\text{Sr} = 0.710249$, which allows for mass bias in the plasma to be fully corrected.

A 28.8 mg aliquot of sample 42R3 24–30 was spiked with a ^{229}Th - ^{233}U mixed tracer and digested in double-distilled nitric acid. U and Th were separated by conventional anion-exchange column chemistry using Bio-Rad AG 1-X8 resin following Clark et al. (2014). The purified U-Th mixed solution was analysed for ^{238}U , ^{234}U , ^{232}Th and ^{230}Th in multi-static mode on the Nu Plasma HR multi-collector ICP-MS at the University of Queensland, following Clark et al. (2014). The samples $^{230}\text{Th}/^{238}\text{U}$ and $^{234}\text{U}/^{238}\text{U}$ activity ratios were calculated using the decay constants given in Cheng et al. (2000) and the U-Th age was calculated using the Isoplot 3.76 Program (Ludwig, 2012).

3. Results

3.1. Trace elements and Sr isotopes

The selected veins are mostly low-Mg calcite with 10,000–14,000 $\mu\text{g/g}$ Mg (1.7–2.3 wt% MgO) and 200–300 $\mu\text{g/g}$ Sr. However, sample 36R1 83/84 contains aragonite with up to 7000–9800 $\mu\text{g/g}$ Sr and calcite with 16,000–88,000 $\mu\text{g/g}$ Mg (Table 1; Fig. S1; Electronic Supplement). The dominant low-Mg calcite veins have Sr/Ca of 0.22–0.35 mmol/mol and Mg/Ca of 44–57 mmol/mol (Electronic Supplement) that are typical of calcite veins formed from low-temperature seawater-derived fluids (Coggon et al., 2010) and do not vary systematically down the hole (Fig. S4).

The majority of veins have total rare earth element concentrations (ΣREE) of ~ 0.1 –1 $\mu\text{g/g}$. The REE patterns resemble seawater in having a relative depletion in light rare earth elements and negative Ce and positive Y anomalies. However, in contrast to seawater, most veins have positive Eu anomalies (Fig. 3). The Y anomaly shows a gradual decrease down the hole (Fig. 4d). The two deepest

Table 1
Summary of U-Pb ages, Sr and clumped isotope data for carbonate veins in IODP Hole U1473A.

Core	Interval (cm)	Depth (mbsf)	Mg	Sr	U	Pb	U-Pb Age ^a	MSWD	⁸⁷ Sr/ ⁸⁶ Sr	$\delta^{13}\text{C}_{\text{calcite}}$	$\delta^{18}\text{O}_{\text{calcite}}$	$\Delta_{47 \text{ calcite}}$	$\delta^{18}\text{O}_{\text{fluid}}$	Temp.
			Mean \pm 2 standard deviations				\pm 95% confidence			Mean \pm 95% confidence level				
			($\mu\text{g/g}$)	($\mu\text{g/g}$)	($\mu\text{g/g}$)	($\mu\text{g/g}$)	(Ma)			(‰) (VPDB)	(‰) (VSMOW)	(‰) (I-CDES)	(‰) (VSMOW)	(°C)
21R1	104-109	181.2								3.07 ± 0.02	33.19 ± 0.04	0.593 ± 0.013	3.0 ± 0.9	25 ± 5
25R2	88-89	218.58	12600 ± 1000	255 ± 37	0.19 ± 0.05	0.004 ± 0.007	7.3 ± 0.9	8.0	0.709073(8)	2.54 ± 0.15	33.54 ± 0.35	0.603 ± 0.013	2.6 ± 0.9	22 ± 4
					0.26 ± 0.17	0.006 ± 0.009	0.6 ± 0.8	(7.4)						
29R4	12-17 cc	259.47	11600 ± 800	207 ± 15	0.15 ± 0.03	0.004 ± 0.004	5.8 ± 0.4	3.8	0.709051(7)	2.56 ± 0.02	33.06 ± 0.04	0.635 ± 0.014	0.1 ± 0.9	12 ± 4
29R4	12-17 cc/sm	259.47					8.2 ± 0.2	2.4						
29R4	102-108	260.35	11100 ± 1100	201 ± 54	0.18 ± 0.11	0.005 ± 0.004	7.4 ± 0.9	(2.4)	0.709044(8)	2.35 ± 0.02	33.58 ± 0.09	0.633 ± 0.015	0.7 ± 1.0	12 ± 5
33R1	57-64	294.37	11200 ± 700	227 ± 24	0.16 ± 0.3	0.006 ± 0.028	8.0 ± 0.2	(1.5)	0.708525(7)	2.81 ± 0.01	32.94 ± 0.04	0.643 ± 0.025	-0.5 ± 1.6	10 ± 7
33R1	107-110	294.87	14000 ± 1900	329 ± 80	0.15 ± 0.03	0.001 ± 0.001	8.8 ± 0.7	4.5		2.88 ± 0.01	33.23 ± 0.04	0.570 ± 0.038	4.5 ± 2.6	33 ± 14
34R3	85-89	306.42					9.7 ± 0.5	4.8						
34R4	4-10	306.85	10000 ± 800	174 ± 25	0.11 ± 0.04	0.02 ± 0.10	8.0 ± 1.9	(12)	0.709039(9)	2.52 ± 0.03	33.06 ± 0.08	0.646 ± 0.020	-0.6 ± 1.2	9 ± 6
36R1	83-84	323.74	26000 ± 52000	290-9750	0.09-1.6	0.001-0.14	10.4 ± 0.3	17		2.69 ± 0.01	33.35 ± 0.04	0.575 ± 0.037	4.3 ± 2.7	32 ± 14
36R3	41-46	326.25	11300 ± 1000	216 ± 38	0.15 ± 0.05	0.005 ± 0.004				2.82 ± 0.05	33.08 ± 0.09	0.617 ± 0.034	1.3 ± 2.2	17 ± 10
42R2	3-4	382.64	13000 ± 2800	260 ± 170	0.10 ± 0.10	0.001 ± 0.003	9.1 ± 0.2	(1.8)		2.55 ± 0.08	33.09 ± 0.16	0.596 ± 0.024	2.7 ± 1.6	24 ± 8
42R3	24-30	382.89	12200 ± 1400	264 ± 66	0.20 ± 0.08	0.02 ± 0.06	1.2 ± 1.2	4.7	0.708772(8)	2.84 ± 0.01	33.10 ± 0.05	0.624 ± 0.020	0.8 ± 1.3	15 ± 6
46R1	51-63	411.32	12500 ± 1900	275 ± 87	0.22 ± 0.10	0.019 ± 0.017	9.6 ± 1.5	7.6	0.708930(8)	2.73 ± 0.03	33.24 ± 0.06	0.641 ± 0.018	-0.1 ± 1.1	10 ± 5
46R1	134-135	412.16	13300 ± 1900	295 ± 69	0.15 ± 0.01	0.006 ± 0.004	9.0 ± 0.4	5.7		2.82 ± 0.02	33.26 ± 0.04	0.628 ± 0.020	0.7 ± 1.3	14 ± 6
47R1	56-57	421.07	13500 ± 1700	297 ± 70	0.15 ± 0.05	0.008 ± 0.006	9.1 ± 1.3	4.6		2.78 ± 0.10	33.36 ± 0.13	0.570 ± 0.043	4.7 ± 3.0	33 ± 17
47R1	93-94	421.42	13000 ± 1600	297 ± 72	0.16 ± 0.06	0.011 ± 0.005	7.6 ± 0.9	5.2		2.87 ± 0.03	33.42 ± 0.05	0.579 ± 0.041	4.1 ± 2.9	30 ± 15
47R1	96-105	421.45	12400 ± 2100	272 ± 88	0.20 ± 0.09	0.012 ± 0.009	8.5 ± 1.8	5.7	0.70903(1)					
50R2	136-137	452.46								2.73 ± 0.04	33.47 ± 0.04	0.616 ± 0.045	1.7 ± 3.0	18 ± 15
51R1	78-85	460.80	12800 ± 2800	282 ± 100	0.18 ± 0.06	0.007 ± 0.015	8.8 ± 0.3	6.8		3.20 ± 0.03	33.05 ± 0.07	0.631 ± 0.016	0.3 ± 1.0	13 ± 5
51R1	127-130	461.27	12800 ± 2900	260 ± 100	0.17 ± 0.05	0.010 ± 0.007	8.0 ± 1.0	3.5						
					0.30 ± 0.13	0.013 ± 0.014	0.1 ± 0.4	(2.5)						
52R1	40-44	469.42	13400 ± 8800	302 ± 290	0.12 ± 0.09	0.009 ± 0.005	10.4 ± 0.7	2.8	0.708954(7)	2.33 ± 0.05	33.36 ± 0.03	0.570 ± 0.028	4.7 ± 1.8	33 ± 10
58R8	31-35	528.50	30000 ± 78000	230 ± 57	0.49 ± 2.05	0.001 ± 0.001	9.2 ± 0.8	(22)	0.708881(8)	2.35 ± 0.08	32.89 ± 0.03	0.596 ± 0.038	2.5 ± 2.4	24 ± 13
61R6	54-59	555.50	12400 ± 1900	269 ± 97	0.15 ± 0.10	0.02 ± 0.02	8.1 ± 1.1	8.6	0.709039(9)	2.49 ± 0.04	33.70 ± 0.09	0.589 ± 0.022	3.7 ± 1.5	27 ± 8
62R2	25-29	616.45	10800 ± 900	192 ± 34	0.16 ± 0.06	0.012 ± 0.017	7.6 ± 0.6	4.1	0.709022(9)	2.85 ± 0.06	32.65 ± 0.10	0.621 ± 0.020	0.6 ± 1.3	16 ± 6
Mean (n = 21)										2.70 ± 0.11	33.22 ± 0.11	0.608 ± 0.012	2.0 ± 0.8	21 ± 4

^a Most preferred ages are based on best fit regressions, where the initial $^{207}\text{Pb}/^{206}\text{Pb}$ ratio is 0.88 ± 0.02 , or the regression forced through the average gabbro $^{207}\text{Pb}/^{206}\text{Pb}$ of 0.88. Note that the U-Th age for sample 42R3 24-30 is 273 ± 5 Ka. MSWDs in brackets are based on limited or selected data. Temperatures calculated based on the Δ_{47} calibration of Anderson et al. (2021). Note all veins are dominated by low-Mg calcite, but aragonite was identified in 36R1 83-84 (Fig. S1). $\delta^{18}\text{O}_{\text{fluid}}$ are minimum values calculated based on the calibration of Daëron et al. (2019) (Table S4 Electronic Supplement).

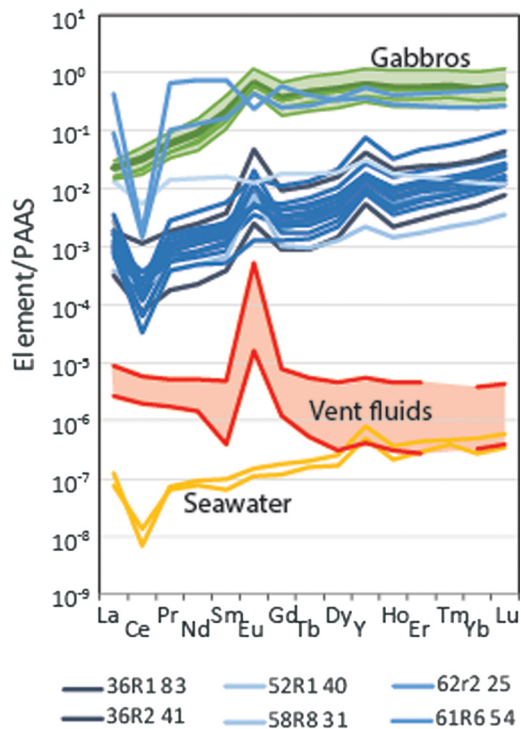


Fig. 3. Carbonate vein rare earth element – yttrium (REY) data (blue) normalised to Post Archean Australian Shale (Pourmand et al., 2012). The compositional ranges of seawater, vent fluids (Fowler et al., 2019 and references therein) and Atlantis Bank Gabbros (green - Hart et al., 1999) are shown for reference.

veins have flat rare earth element patterns, very strongly negative Ce anomalies and high total rare earth element concentrations (ΣREE) in the 10–100 $\mu\text{g/g}$ range (Fig. 3).

The $^{87}\text{Sr}/^{86}\text{Sr}$ ratios measured in twelve veins vary from 0.70853 to 0.70907 (Table 1). The majority of the veins have $^{87}\text{Sr}/^{86}\text{Sr}$ ratios close to seawater values that have varied from 0.7088 at 12 Ma to the modern value of 0.7092. However, two veins have $^{87}\text{Sr}/^{86}\text{Sr}$ ratios of significantly less than seawater (Figs. 4e and S5; McArthur et al., 2001).

3.2. U–Pb ages

Most of the veins investigated ($n = 21/22$) have average concentrations of 0.1–0.2 $\mu\text{g/g}$ U and 0.001–0.02 $\mu\text{g/g}$ Pb, with a higher average concentration of 0.5 $\mu\text{g/g}$ U in sample 58R8 31–35 (Table 1). The precision of the $^{238}\text{U}/^{206}\text{Pb}$ and $^{207}\text{Pb}/^{206}\text{Pb}$ ratios measured in individual spots varies from the 1–2% level to tens of percent depending on the U-content and the homogeneity of the carbonate ablated. The plotted data have been filtered to remove analyses with uncertainties of more than 8% in the $^{238}\text{U}/^{206}\text{Pb}$ ratio and 10% in the $^{207}\text{Pb}/^{206}\text{Pb}$ ratio. The remaining analyses shown in Fig. 5 have $^{238}\text{U}/^{206}\text{Pb}$ ratios that vary from close to zero to more than 600 and are correlated with $^{207}\text{Pb}/^{206}\text{Pb}$ to varying degrees.

Half of the veins analysed yield fairly simple correlations with regressions that give MSWDs of ~ 1.8 to 6 (Fig. 5). These samples have an average initial $^{207}\text{Pb}/^{206}\text{Pb}$ ratio of 0.88 that is indistinguishable from the average initial value of the host gabbros of 0.876 ± 0.020 (Hart et al., 1999). These samples include both the youngest and the oldest U–Pb vein ages of 1.2 ± 1.2 Ma and 10.4 ± 0.7 Ma (Table 1). An aliquot of the youngest sample 42R3 24–30 was analysed for short-lived ^{230}Th and ^{234}U by bulk methods and gave a U–Th disequilibrium age of 273 ± 5 Ka (Table S1). Therefore taken together the U–Pb and U–Th data unequivocally

demonstrate that carbonation of the Atlantis Bank seafloor has encompassed a period of at least 10 Myr (Table 1).

The remaining samples are more difficult to interpret. Vein samples 25R2 88–89 and 51R1 127–130 have two regressions each shown in black and red in Fig. 5. The data defining each regression came from discrete domains within the samples (Figs. 2 and S6) demonstrating that at least some of the veins investigated were reactivated more than once and formed by multi-stage growth over several millions of years. For example, the analyses of carbonate distal to the vug in 51R1 127–130 define an age of 8.0 ± 1.0 Ma, whereas the analyses next to the vug define a modern age of 0.1 ± 0.4 Ma (Figs. 2 and 5). Several of the other samples have similar data distributions but the black and blue data ellipses cannot be confidently assigned to discrete domains within the samples. In these cases a single regression is shown for the black ellipses in each sample to represent the most likely original formation age of the sample. The blue ellipses are outliers and could reflect either later carbonate growth or Pb-loss, which moves data points to higher $^{238}\text{U}/^{206}\text{Pb}$ ratios in the concordia diagrams (Fig. 5).

In most cases, the preferred U–Pb ages for each sample (Table 1) represent the best-fit ages where the best-fit $^{207}\text{Pb}/^{206}\text{Pb}$ intercept value is 0.086–0.90, or the age obtained by forcing the regression through the mean gabbro $^{207}\text{Pb}/^{206}\text{Pb}$ ratio of 0.88 (Hart et al., 1999). However, exceptions were made for the young samples (29R4 12–17 and 42R3 24–30), which are expected to have lower more evolved $^{207}\text{Pb}/^{206}\text{Pb}$ intercept values (Fig. 5). In most cases the different approaches give ages within uncertainty of one another, and the choice does not significantly impact the overall distribution of ages. The preferred ages in Table 1 are plotted as a function of depth in the crust, and in relative probability and cumulative frequency diagrams in Fig. 6. The majority of carbonate growth (20/24 episodes including two ages each for 51R1 127–130 and 25R2 88–89) grew in three or four pulses between ~ 10.4 and 7.3 Ma (Fig. 6b). Additional carbonate veining occurred at 5.8 ± 0.4 Ma ($n = 1$) and in the last 1 Ma, evidenced by 3/24 discrete episodes of vein growth (Figs. 5 and 6b; Table 1).

3.3. Clumped O and C isotopes

The 21 calcite veins analysed for clumped isotopes have fairly similar $\delta^{13}\text{C}$, $\delta^{18}\text{O}_{\text{calcite}}$ and Δ_{47} signatures that do not vary systematically as a function of depth (Fig. 4g–i) and define a single cluster in the $\delta^{13}\text{C}$ and $\delta^{18}\text{O}_{\text{calcite}}$ cross plot (Fig. 7). The uncertainties associated with individual analyses are related to the number of sample replicates (Electronic Supplement) and are generally smaller for the more recent analyses undertaken with the 253 Plus instrument rather than the MAT253. The mean values and 95% confidence limits are $2.7 \pm 0.1\text{‰}$ (VPDB) for $\delta^{13}\text{C}$ and $33.2 \pm 0.1\text{‰}$ for $\delta^{18}\text{O}_{\text{calcite}}$ (VSMOW), which are at the upper end of the range previously reported for calcite and aragonite in Hole 735B (Fig. 7; Bach et al., 2001). The high $\delta^{18}\text{O}_{\text{calcite}}$ values would correspond to temperatures of less than 5°C when calculated assuming typical seawater $\delta^{18}\text{O}_{\text{fluid}}$ and using the calibration of Daëron et al. (2019). In contrast, the mean Δ_{47} of $0.611 \pm 0.006\text{‰}$ I-CDES gives a mean formation temperature of $21 \pm 4^\circ\text{C}$, based on the calibration of Anderson et al. (2021). The higher temperature based on the Δ_{47} calibration results in calculated $\delta^{18}\text{O}_{\text{fluid}}$ values with a mean of $2.0 \pm 0.8\text{‰}$ (VSMOW) that is slightly higher than seawater (Fig. 4f; Table 1).

Due to the relatively large uncertainty in the Δ_{47} value of individual samples, and because most of the veins formed in a relatively short ~ 3.1 Ma period between ~ 10.4 and 7.3 Ma, it is not possible to confidently identify systematic changes in the clumped isotope temperature as a function of U–Pb age.

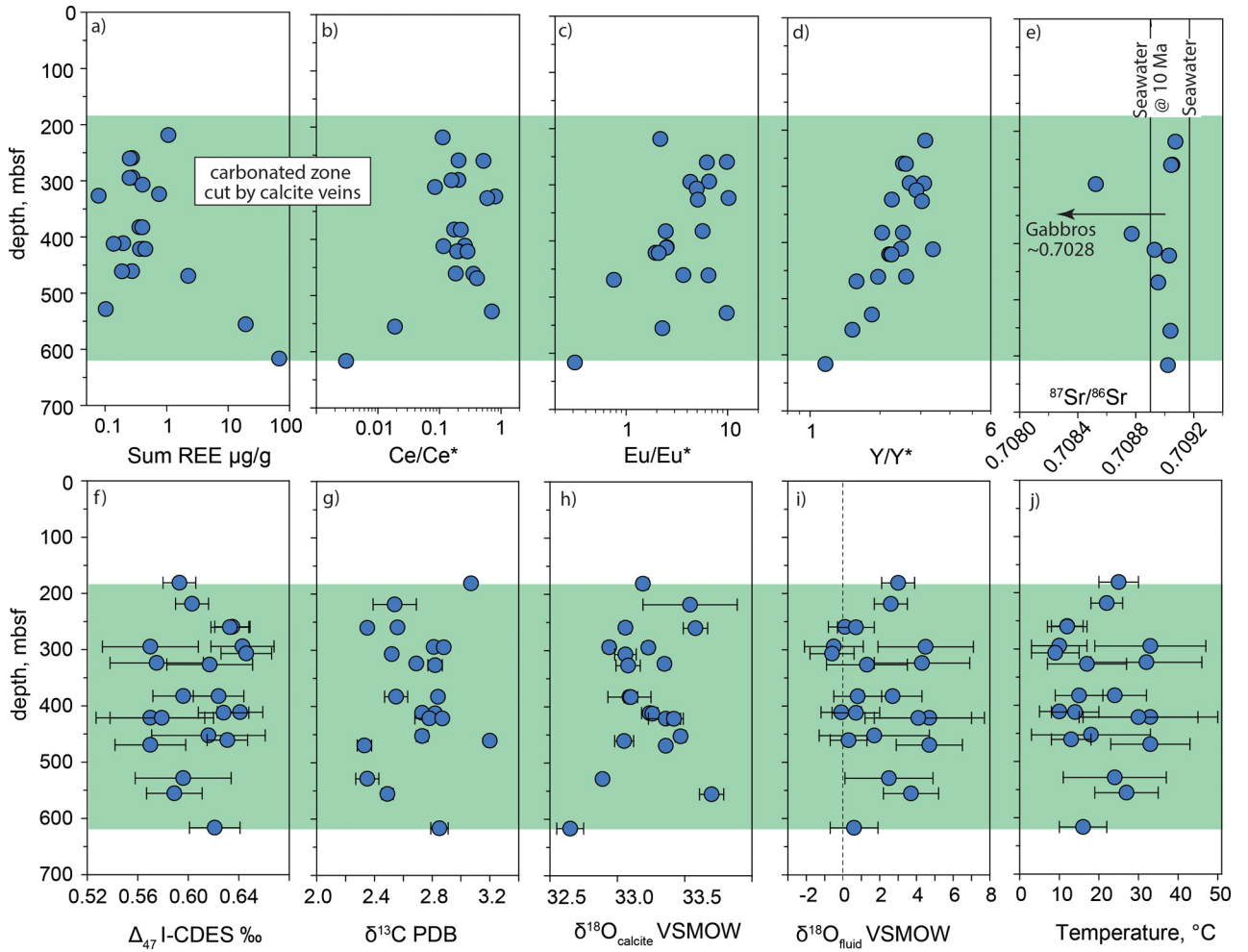


Fig. 4. Variations in carbonate vein chemistry down Hole U1473A, the carbonated zone cut by carbonate veins is shaded green. a) Sum of REE; b) $Ce/Ce^* = Ce_N / (Pr_N * Pr_N / Nd_N)$; c) $Eu/Eu^* = Eu_N / (Sm_N * (Sm_N / Nd_N)^{1/2})$; d) $Y/Y^* = Y_N / (Ho_N * Ho_N / Er_N)$; e) $^{87}Sr/^{86}Sr$; f) Δ_{47} I-CDES ‰; g) $\delta^{13}C$ PDB ‰; h) $\delta^{18}O_{calcite}$ VSMOW ‰; i) $\delta^{18}O_{fluid}$ VSMOW ‰ based on the calibration of Daëron et al. (2019); and j) temperature °C calculated from Δ_{47} based on the calibration in Anderson et al. (2021). Uncertainties represent the 95% confidence level.

4. Discussion

4.1. Atlantis Bank exhumation and cooling history

The calcite vein Δ_{47} formation temperatures and U-Pb ages are shown with previous thermochronological constraints and conductive cooling curves for 12 Ma crust formed at different depths (Fig. 8). The cooling curves were calculated using the relationship $T = T_{mantle} \text{erf}[z/2\sqrt{(\kappa t)}]$, where erf is the error function, T is in °C, T_{mantle} is 1350 °C, depth (z) is in m, the thermal diffusivity (κ) has a value of $10^{-6} \text{ m}^2 \text{ s}^{-1}$ and t is in s (Stein and Stein, 1992).

The carbonate veins formed before 7 Ma have a mean temperature of $21 \pm 4^\circ\text{C}$ that is indistinguishable from the mean of all samples (Table 1) and is higher than modern fluids emanating from fractures in Hole U1473A, which have a poorly defined temperature of $<15^\circ\text{C}$ (MacLeod et al., 2017). The range of temperatures is consistent with those predicted for conductively cooled crust at depths of 200–600 mbsf (Fig. 8). In contrast, the ~12 Ma zircons with Ti-in-zircon temperatures of $\sim 800 \pm 50^\circ\text{C}$ (Rioux et al., 2016), and the biotites with Ar-Ar ages of ~11.4 Ma and nominal closure temperatures of $350 \pm 50^\circ\text{C}$ (John et al., 2004), plot on a cooling curve consistent with crust formed at depths of 2000–2500 m (Fig. 8a). Note that these depth ranges approximate the depths from which the carbonate veins were recovered from Hole U1473A and the probable depth of gabbro accretion at ~2000–2500 mbsf (Fig. 8; Vanko and Stakes, 1991; Dick et al., 2019).

Taken together the combined U-Pb zircon, Ar-Ar biotite and carbonate U-Pb ages and corresponding temperatures are consistent with a simple cooling and exhumation history in which: i) the felsic veins and oxide gabbros were emplaced at $\sim 800 \pm 50^\circ\text{C}$ at 2500–2000 mbsf at ~12 Ma; ii) the gabbros were rapidly cooled to $\sim 350^\circ\text{C}$ by ~11.4 Ma ($\sim 830^\circ\text{C/Myr}$); iii) the gabbros were exhumed to a depth of 200–600 mbsf, and cooled to $21 \pm 4^\circ\text{C}$ by 10.4 ± 0.3 Ma ($330 \pm 200^\circ\text{C/Myr}$); iv) the gabbros continued slow cooling and carbonate vein growth from 10.4 ± 0.3 Ma until ~7 Ma, with renewed vein growth in recent times (Fig. 8 and references therein).

The new data do not favour the previously proposed cooling model in which a sill intruded at ~9.4 Ma generating a 250°C thermal pulse that reset the U/Th-He and fission track ages (John et al., 2004; Schwartz et al., 2009). Clumped isotope reordering models (e.g. Stolper and Eiler, 2015) evaluated with the Clumpy-Cool (Lloyd, 2020) and Isotopylog (Hemingway and Henkes, 2021) packages for python, indicate there is no realistic scenario under which the observed low clumped isotope formation temperatures of around 20°C could be preserved if the samples were exposed to high temperatures after formation. Several scenarios were considered including one similar to the cooling history proposed by Schwartz et al. (2009) in which the crust cooled to 25°C and was then subjected to a 250°C heat pulse at 9.5 Ma, and cooled back to 25°C over a million years. All the scenarios tested resulted in

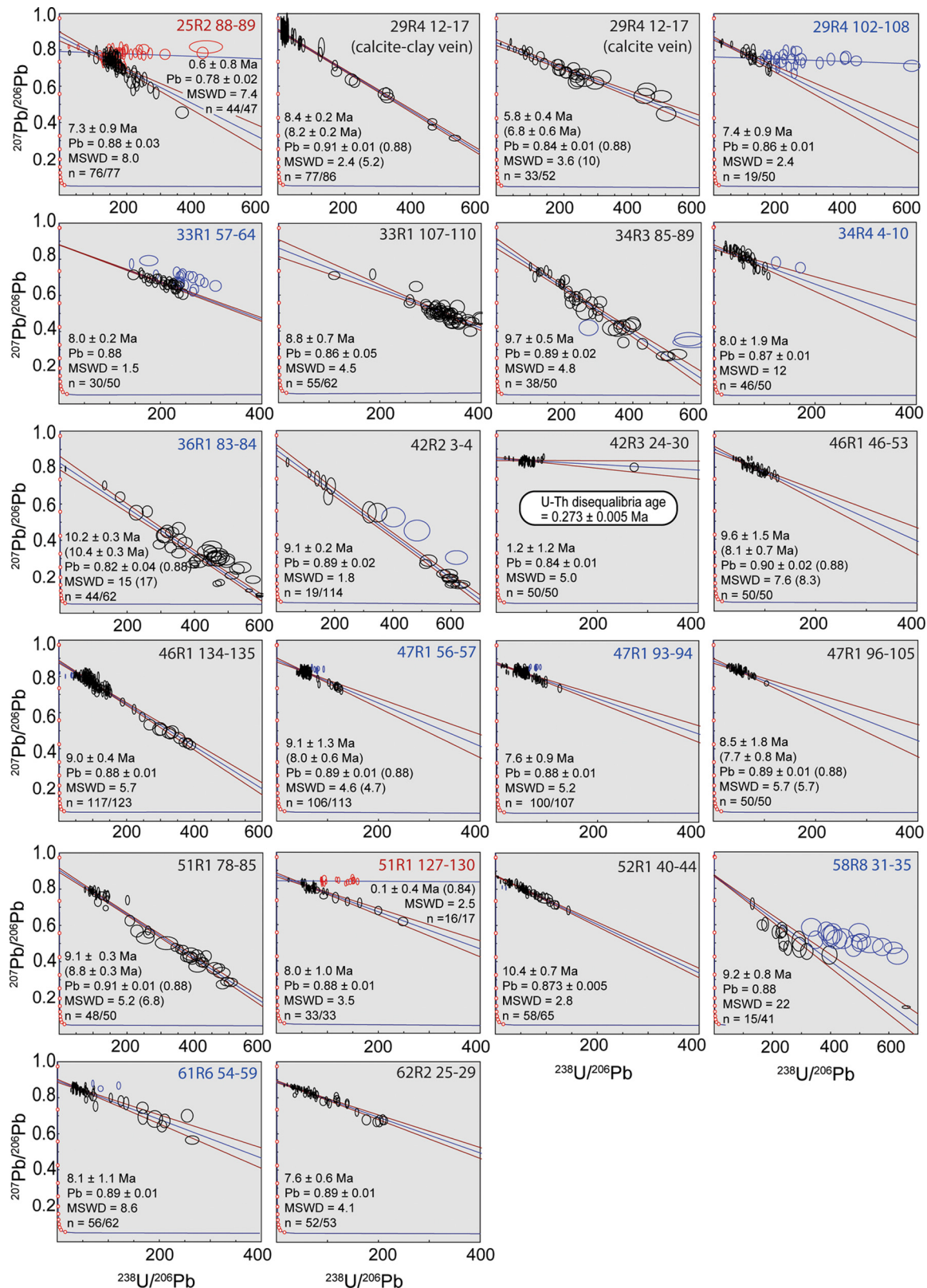


Fig. 5. Tera-Wasserburg concordia diagrams showing laser analyses of carbonate veins recovered from Hole U1473A. Note that a calcite vein and calcite-clay vein in 29R4 12-17 are plotted separately, but different domains within the veins in samples 25R2 88-89 and 51R1 127-130 are distinguished by colour on the same diagram (see Fig. 2). The ages and uncertainties (95% confidence level) were calculated using Model 1 regressions in Isoplot 3.76 and include the Student's-t multiplier (Ludwig, 2012). The best fit $^{207}\text{Pb}/^{206}\text{Pb}$ intercepts (denoted Pb =) are given; values in parentheses are for regressions forced through a $^{207}\text{Pb}/^{206}\text{Pb}$ of 0.88. The U-Th age is reported in Table S1.

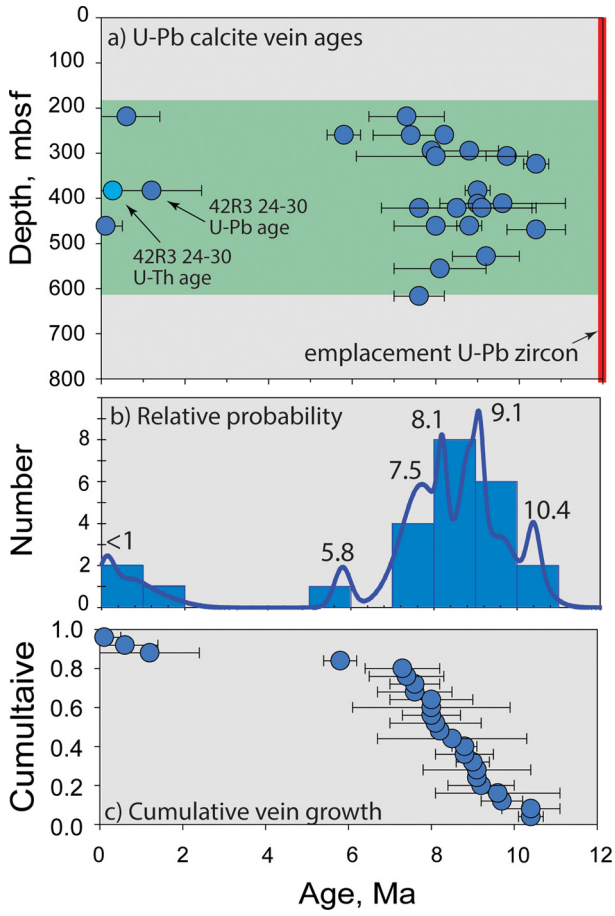


Fig. 6. Summary of U-Pb ages obtained from Tera-Wasserburg plots for carbonate veins in IODP Hole U1473A and the U-Th age for sample 42R3 24-30 (Fig. 5; Table S1). a) The U-Pb and U-Th ages versus depth in the drill hole (metres below seafloor – mbsf) with the ~ 12.0 Ma emplacement age shown for reference (Rioux et al., 2016). b) Histogram and relative probability of age distribution showing peaks in calcite vein growth at ~ 10.4 , ~ 9.1 , ~ 8.1 , ~ 7.5 , ~ 5.8 and <1 Ma. c) Cumulative vein growth by age. Note 24 ages for carbonate in 22 veins are shown (Table 1). Uncertainties represent the 95% confidence level.

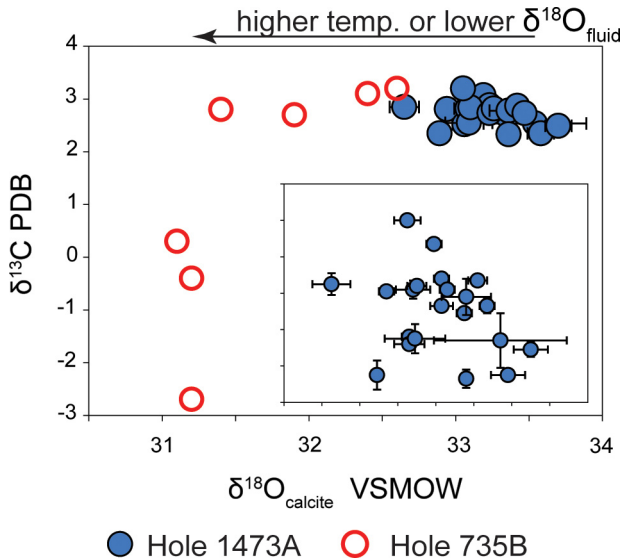


Fig. 7. $\delta^{18}\text{O}_{\text{calcite}}$ VSMOW versus $\delta^{13}\text{C}$ PDB for calcite and aragonite veins from Hole 1473A (Table 1) and Hole 735B (Bach et al., 2001). The tick marks on the inset graph enlarging Hole U1473A data represent intervals of 0.2‰ .

reordering of the clumped isotopes and final Δ_{47} values of much lower than the measured values. Therefore the combined Δ_{47} and U/Pb data do not favour a thermal pulse after 10.4 ± 0.3 Ma (see Fig. S7).

The simplest way to reconcile the cooling histories suggested by the carbonate veins and traditional thermochronometers is through the uncertainties associated with the ages. The analytical uncertainty and distribution of individual laser spot analyses in Fig. 5 provide confidence that the carbonate veins formed in several distinct episodes of vein growth with the first major phase marked by veins with ages of 10.4 ± 0.3 Ma and 10.4 ± 0.7 Ma (Fig. 6bc). These vein ages suggest the crust had cooled to the mean Δ_{47} temperature of $21 \pm 4^\circ\text{C}$ by at least 10.1 Ma and possibly as early as 11.1 Ma (Fig. 8). In contrast, the 19 unique U/Th-He zircon ages reported by Schwartz et al. (2009) have relatively high uncertainties and define a wide distribution with a single mode at $9.4^{+1.1}_{-0.6}$ Ma (Fig. 8c). This age is similar to the central fission-track ages reported for zircon (John et al., 2004) and we interpret it as representing a single cooling event related to exhumation. The upper limit of this age at 10.5 Ma is within uncertainty of the oldest carbonate vein ages of 10.4 ± 0.3 Ma and 10.4 ± 0.7 Ma. Therefore the combined data are consistent with the crust cooling through the U/Th-He closure temperature by ~ 10.5 Ma and to $21 \pm 4^\circ\text{C}$ by ~ 10.1 Ma (Fig. 8).

The Atlantis Bank occurs in the footwall of a detachment fault, and current models suggest it formed by continuous extension on a detachment fault that soled into an active intrusion zone undergoing crystal plastic deformation (Dick et al., 2000, 2019). The rate of exhumation in this scenario depends on the geometry of the detachment fault as well as the rate of movement on the detachment, which has been estimated as 14 mm/Myr at the time of gabbro emplacement (Baines et al., 2008). Exhumation probably began immediately after initial emplacement of the gabbros at depths of greater than ~ 2000 – 2500 mbsf (Vanko and Stakes, 1991), with exhumation to their current position following immediately afterwards (cf. Fig. 8). The formation of the earliest carbonate veins at 10.4 ± 0.3 Ma and 10.4 ± 0.7 Ma, in crust that was ~ 1.6 Myr old, indicates broadly similar timing to other core complexes. On the Mid-Atlantic Ridge, ~ 1.2 Ma gabbros were exhumed on the Atlantis Massif over a period of ~ 1 Myr and carbonation of metagabbros and peridotites has occurred in the last 50,000 yrs (Ternieten et al., 2021). The core complex exhuming ~ 1.5 Ma seafloor at ODP Site 1271 close to the $15^\circ 20'$ Fracture Zone, has also been carbonated in the last 130,000 years (Bach et al., 2011).

4.2. Oceanic core complex carbonation rates

The average concentration of carbon in Atlantis Bank gabbroic crust expressed as wt% oxide is estimated here as 0.15 ± 0.04 wt% CO_2 made up of 0.02 ± 0.01 wt% CO_2 in carbonate veins and 0.13 ± 0.04 wt% CO_2 in wall-rock alteration (Fig. 9).

Carbonate veins are estimated to contribute 0.02 ± 0.01 wt% CO_2 based on the logged frequency of veins from Holes U1473A and 735B (Natland et al., 2002; MacLeod et al., 2017). The ~ 800 -m deep Hole U1473A core is estimated to contain an average of 0.06 vol% carbonate veins based on the average vein thickness of 1.2 mm and average frequency of 5 per 10 m (MacLeod et al., 2017). In comparison, the upper 800 m of Hole 735B has a lower estimated abundance of 0.03 vol% (Natland et al., 2002). The abundance of veins is highly variable, even within Hole U1473A (Fig. 9a), however, these figures indicate an average concentration of 0.02 ± 0.01 wt% CO_2 in carbonate veins in the upper 800-m of Atlantis Bank crust.

Altered gabbros host carbonate intergrown with Fe-oxyhydroxide alteration, replacing olivine and in microveinlets (Bach et al., 2001; Dick et al., 2019; Kendrick, 2019; Kendrick et al., 2020a).

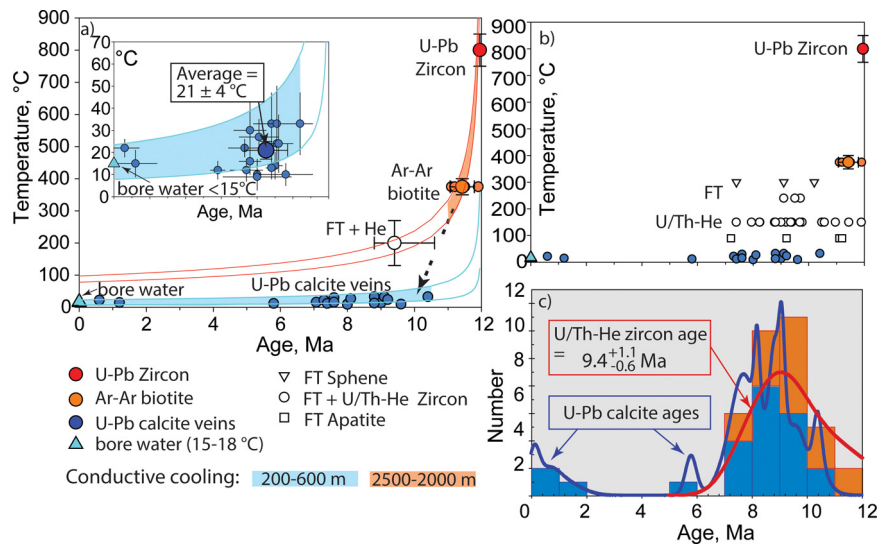


Fig. 8. a) The U-Pb ages and clumped isotope temperatures of Hole U1473A carbonate veins are plotted together with published U-Pb zircon, Ar-Ar biotite ages (John et al., 2004) and the median zircon U-Th-He age (see part c). Curves are shown for conductive cooling of crust emplaced at different depths based on Stein and Stein (1992). The inset shows an enlargement of the carbonate vein data. b) Published U-Pb zircon, Ar-Ar biotite, Fission Track and U/Th-He data (John et al., 2004; Schwartz et al., 2009; Rioux et al., 2016). c) Cumulative probability curves and stacked histograms for the U-Pb carbonate ages (blue - Table 1) and U/Th-He ages (red - Schwartz et al., 2009). Uncertainties represent the 95% confidence level.

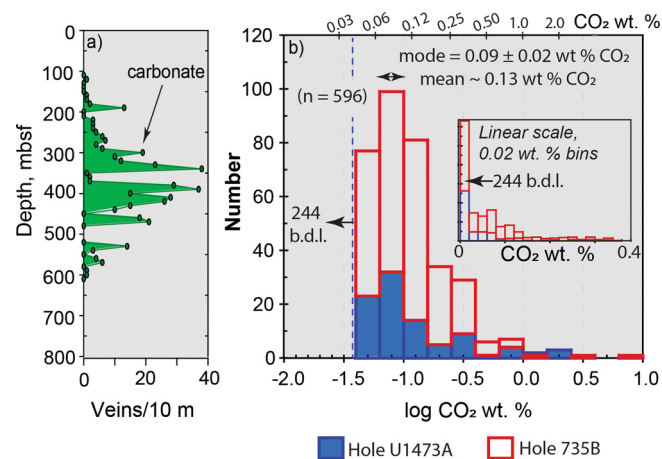


Fig. 9. a) The frequency of carbonate veins in Hole U1473A and b) a histogram of log CO₂ wt.% in whole rock sample powders from Holes 1473A and 735B (Bach et al., 2001; Natland et al., 2002; MacLeod et al., 2017). The mode represents the minimum likely CO₂ concentration, the mean is estimated as 0.13 wt.% CO₂ assuming samples with CO₂ below the detection limit contain 0.02 wt.% CO₂. Uncertainties represent the 95% confidence level. b.d.l. = below detection limit.

Shipboard analyses indicate whole rock CO₂ concentrations range from below the quoted detection limits of 0.03–0.05 wt.% CO₂ up to 0.67 wt.% CO₂ in Hole 735B (Natland et al., 2002) and up to 2.7 wt.% CO₂ in Hole U1473A (MacLeod et al., 2017), with even higher values of up to 8.1 wt.% CO₂ reported for post-cruise analysis of altered samples (Bach et al., 2001). The mean whole rock concentration of CO₂ can be estimated as ~0.13 wt.% CO₂, assuming samples with CO₂ below the quoted detection limits of 0.03–0.05 wt.% CO₂ contain 0.02 wt.% CO₂. The mean changes by only 0.01 wt.% CO₂ if these samples contain either 0.00 wt.% CO₂ or 0.05 wt.% CO₂. However, we adopt a mean value of 0.13 ± 0.04 wt.% CO₂, which contains a more conservative estimate of uncertainty that allows for possible sampling biases. The uncertainty here is based on the observation that CO₂ concentration data follow a log-normal distribution that is typical of many trace elements (Fig. 9). The mode of these data is relatively well defined and represents the minimum possible value for mean CO₂ concentration.

The estimated bulk crustal concentration of ~0.15 ± 0.04 wt.% CO₂ in veins and the rock matrix is at the lower end of the range

of 0.14–0.5 wt.% CO₂ reported for ~6 Ma basalts in ODP Holes 504B and 896 from near to the East Pacific Rise (Alt and Teagle, 1999), and broadly similar to gabbros exposed in other ocean core complexes. Gabbros in the 15°45′ core complex (ODP Site 1275) host ~0.01 vol.% carbonate veins that is ~3–6 times less than the Atlantis Bank (above); however, these gabbros were emplaced at ~2–2.5 Ma meaning there has been a shorter period for carbonation (Schroeder et al., 2015). Shipboard analyses of ~1.3 Ma gabbros and troctolites exposed in Hess Deep Rift indicate CO₂ contents comparable to the Atlantis Bank gabbros despite their younger age (Gillis et al., 2014). In comparison, troctolites in the 15°45′ core complex have much higher abundances of carbonate veins and alteration than nearby gabbros (Schroeder et al., 2015).

Comparing the CO₂ content of different drill holes requires an allowance to be made for crustal age or that we consider average carbonation rates. By combining the U-Pb ages for carbonate veins on the Atlantis Bank and the estimated crustal concentration of ~0.15 ± 0.04 wt.% CO₂ we can begin to evaluate changes in carbonation rate on the Atlantis Bank (Fig. 6). Most of the 22 veins

investigated from the Atlantis Bank originally formed over a period of 3.1 ± 1.1 Myr between $\sim 10.4 \pm 0.7$ Ma and $\sim 7.3 \pm 0.9$ Ma (Fig. 6c). If crustal carbonation occurred proportionally with vein growth, $\sim 83 \pm 8\%$ of the crustal carbonate (e.g. 20/24 vein growth events in Table 1) formed during a 3.1 ± 1.1 Myr period, which indicates an initial carbonation rate of $\sim 400 \pm 200$ $\mu\text{g/g}$ per Myr. The carbonation rate then decreased to a very low level, with a single vein forming between 7 Ma and ~ 1 Ma (Fig. 6b), before carbonation resumed in the last ~ 1 Ma (Fig. 6b). Carbonation in the last 1 Ma is recorded by sample 42R3 24-30 and new growth zones in samples 25R2 88-89 and 51R1 127-130 (Figs. 2 and 5). Unfortunately, the timing of these events cannot be precisely constrained by the U-Pb method: it could have spanned as little as 0.27 Ma, based on the U-Th age for sample 42R3 24-30 or more than 1 Myr based on the upper uncertainty limit of the young U-Pb age for sample 25R2 88-89 (Fig. 5; Electronic supplement). Assuming this recent vein growth accounts for $\sim 13 \pm 4\%$ of the total carbonation (based on 3/24 vein growth events) the modern carbonation rate could be similar to the original rate of ~ 400 $\mu\text{g/g}$ per Myr or significantly lower.

Further geochronological studies of veins and wall-rock alteration are clearly required to reduce the large uncertainties in the estimated carbonation rates. The estimated carbonation rate on the Atlantis Bank could change if a large number of additional veins, including samples with different $\delta^{13}\text{C}$ and $\delta^{18}\text{O}$ (Fig. 7), were found to have ages of less than 7 Ma (cf. Fig. 6). However, the apparently episodic nature of carbonation in Hole 1473A (Fig. 6b), is not surprising and probably relates to fault dilation during uplift and exhumation of the Atlantis Bank and reactivation during subsequent subsidence or as a result of changes in plate motion.

The renewed carbonation of Hole 1473A in the last 1 Ma (~ 11 Myr after crustal accretion), is consistent with crustal carbonation continuing for as long as seawater-derived fluids can access the crust (e.g. Alt and Teagle, 1999). Given that oceanic core complexes are bathymetric highs that are less likely to be covered by sediments than typical basaltic crust, and oceanic core complexes form on deeply-penetrating detachment faults that provide high permeability pathways, and some oceanic core complexes expose reactive troctolitic or peridotitic lithologies, oceanic core complexes are likely to be important sites of long-lived alteration on the seafloor.

4.3. Unusual alteration fluids?

The calcite veins on the Atlantis Bank are indicated to have formed at an average temperature of $21 \pm 4^\circ\text{C}$ from seawater-derived fluids. The involvement of seawater is indicated because most of the veins are dominated by seawater Sr (Fig. 4e), have $\delta^{13}\text{C}$ of $2.7 \pm 0.1\text{‰}$ that is in the range of carbonate precipitated from seawater (Fig. 4g), and they preserve REE patterns reminiscent of their seawater source (Fig. 3). In contrast with seawater, the calcite veins preserve positive Eu anomalies (Fig. 3) that demonstrate interaction with either the basement lithologies or a volumetrically minor hydrothermal fluid. Due to the much higher Eu content of hydrothermal vent fluids compared to seawater (Fig. 3) the Eu/Eu* anomalies could be explained by the involvement of as little as 0.1–1 vol.% of a typical hydrothermal vent fluid. Similarly, the $^{87}\text{Sr}/^{86}\text{Sr}$ values of slightly less than seawater in samples 33R1 57-64 and 42R3 24-30, which come from 295–383 mbsf, just above a major fault zone (Fig. 4e; Dick et al., 2019), might be explained by either fluid-rock reactions or input of a hydrothermal fluid. Overall, the Sr and rare earth element characteristics of the veins are similar to those reported for other low-temperature carbonate veins in oceanic core complexes previously (Eickmann et al., 2009; Bach et al., 2011; Schroeder et al., 2015).

One geochemical parameter that is unexpected is the calculated range of $\delta^{18}\text{O}_{\text{fluid}}$ values (Fig. 4i; Table 1). The lowest $\delta^{18}\text{O}_{\text{fluid}}$ val-

ues calculated using the calibration of Daëron et al. (2019) are within uncertainty of the expected 0‰ seawater value. However, the maximum $\delta^{18}\text{O}_{\text{fluid}}$ value of $4.7 \pm 1.8\text{‰}$ is significantly higher than seawater at the 95% confidence level (Fig. 4i) and even higher $\delta^{18}\text{O}_{\text{fluid}}$ values are implied by alternative oxygen isotope calibrations (Kim and O'Neil, 1997; Table S5 Electronic Supplement). Most previous studies have assumed that low-temperature carbonation fluids have seawater $\delta^{18}\text{O}$ signatures (Eickmann et al., 2009; Bach et al., 2011; Schroeder et al., 2015). A single previous study applied clumped isotopes to 20 carbonate veins recovered from the Atlantis Massif core complex, demonstrating a mean $\delta^{18}\text{O}_{\text{fluid}}$ of $1.5 \pm 2\text{‰}$ that is indistinguishable from seawater, but with a range of -1.09 to $+5.35\text{‰}$ (Ternieten et al., 2021). Nonetheless, the full range of $\delta^{18}\text{O}_{\text{fluid}}$ in low-temperature alteration fluids is not yet known.

Fluids with positive $\delta^{18}\text{O}_{\text{fluid}}$ are usually attributed to high temperature alteration of fresh ocean crust (e.g. Alt and Bach, 2006) or magmatic sources. However, many of the veins in the current study formed a few million years after accretion of the Atlantis Bank meaning that fluids originally involved in high-temperature alteration or exsolved from felsic veins during accretion are not expected to have been preserved within the crust. It is also difficult to envisage a mixing scenario that could result in positive $\delta^{18}\text{O}_{\text{fluid}}$ values without also overprinting the $^{87}\text{Sr}/^{86}\text{Sr}$ and rare earth element signatures that are so reminiscent of seawater (e.g. Figs. 3 and 4e). Alternative possibilities might be that the positive $\delta^{18}\text{O}_{\text{fluid}}$ values were generated by multi-stage processes at low but evolving temperatures or by specific fluid-mineral reactions. We eagerly anticipate future studies that will improve constraint on the range of $\delta^{18}\text{O}_{\text{fluid}}$ in low-temperature alteration fluids and enable the emergence of a more satisfactory and complete explanation for the observed $\delta^{18}\text{O}_{\text{fluid}}$ values.

5. Conclusions

The combination of laser ablation U-Pb dating, U-Th disequilibrium dating for young samples, clumped isotope, Sr-isotope and trace element analyses of calcite veins in the oceanic basement can provide a wealth of information about the timing of fluid-related processes and carbonation of the ocean crust.

The gabbros exposed on the Atlantis Bank began exhumation from more than 2500 mbsf, immediately after emplacement at ~ 12 Ma. The carbonate vein data indicate the gabbro basement had been exhumed close to its current depth below the seafloor, and cooled to $21 \pm 4^\circ\text{C}$ by 10.4 ± 0.3 Ma.

Combining the age data with an estimated bulk crustal concentration of 0.15 ± 0.04 wt.% CO_2 , we estimate an initial carbonation rate of 400 ± 200 $\mu\text{g/g}$ CO_2 per Myr between $\sim 10.4 \pm 0.7$ Ma and 7.3 ± 0.9 Ma. A single vein formed in the interval 7.3 Ma to 1 Ma suggesting a virtual hiatus in carbonation. However, renewed carbonation recommenced at a poorly defined rate possibly as high as ~ 400 $\mu\text{g/g}$ CO_2 per Myr in the last 0.27–1 Ma. These carbonation rates are indicative averages for periods of hundreds-of-thousand to a few million years based on a relatively small number of samples. Therefore, episodic carbonation could have proceeded at much higher rates over short intervals within the major phases of carbonation at 10.4–7.3 Ma and < 1 Ma (Fig. 6b).

Carbonation is strongly controlled by fluid infiltration. We suggest that because oceanic core complexes are bathymetric highs that accumulate less sediment than typical crust, and because they form on crustal-scale detachment faults that provide high permeability pathways, core complexes like the Atlantis Bank have the potential to become important sites of crustal alteration in crust older than ~ 10 –20 Myr.

CRediT authorship contribution statement

Kendrick and Plümper collected the samples during IODP expedition 360 and conceived different aspects of the study. Kendrick undertook LA-ICPMS analyses together with Yuexing Feng. Kendrick, Feng and Zhao participated in U-Pb data reduction and age interpretation. Plümper and Müller undertook or supervised clumped isotope analyses with oversight from Ziegler. Kendrick synthesised the datasets and wrote the manuscript with input from Plümper, Defliese and Ziegler. All authors contributed to the final interpretation and editing of the manuscript.

Declaration of competing interest

The authors declare that they have no known competing financial interests or personal relationships that could have appeared to influence the work reported in this paper.

Acknowledgements

Ai Nguyen, Gang Xia, Faye Liu and Wei Zhou are gratefully acknowledged for technical assistance in the Sample Preparation and Radiogenic Isotope Facility laboratories at the University of Queensland. We thank the International Ocean Discovery Program (IODP) and the Australia-New Zealand IODP Consortium (ANZIC), which enabled Kendrick to participate on Exp 360. ANZIC is supported by the Australian Government through the Australian Research Council's LIEF funding scheme [LE160100067] and the Australian and New Zealand consortium of universities and government agencies. Martin Ziegler and Inigo A. Müller would like to acknowledge the NWO for support for the clumped isotope analysis with the VIDI grant WE.267002.1. Oliver Plümper acknowledges a NWO Veni grant (863.13.006) and an ERC starting grant "nanoEARTH" (852069). Kirsten Roetert Steenbruggen is thanked for the help with the clumped isotope analysis. We gratefully acknowledge the constructive comments of three anonymous reviewers and the editor (Laurence Coogan), which significantly improved the presentation and focus of this manuscript.

Appendix A. Supplementary material

Supplementary material related to this article can be found online at <https://doi.org/10.1016/j.epsl.2022.117474>.

References

- Alt, J.C., Bach, W., 2006. Oxygen isotope composition of a section of lower oceanic crust, ODP Hole 735B. *Geochem. Geophys. Geosyst.* 7.
- Alt, J.C., Teagle, D.A.H., 1999. The uptake of carbon during alteration of ocean crust. *Geochim. Cosmochim. Acta* 63, 1527–1535.
- Anderson, N.T., Kelson, J.R., Kele, S., Daëron, M., Bonifacie, M., Horita, J., et al., 2021. A unified clumped isotope thermometer calibration (0.5–1,100 °C) using carbonate-based standardization. *Geophys. Res. Lett.* 48, e2020GL092069. <https://doi.org/10.1029/2020GL092069>.
- Bach, W., Alt, J.C., Niu, Y., Humphris, S.E., Erzinger, J., Dick, H., 2001. The geochemical consequences of late-stage low-grade alteration of lower ocean crust at the SW Indian Ridge: results from ODP Hole 735B (Leg 176). *Geochim. Cosmochim. Acta* 65, 3267–3287.
- Bach, W., Rosner, M., Jons, N., Rausch, S., Robinson, L.F., Paulick, H., Erzinger, J., 2011. Carbonate veins trace seawater circulation during exhumation and uplift of mantle rock: results from ODP Leg 209. *Earth Planet. Sci. Lett.* 311 (3–4), 242–252.
- Baines, A.G., Cheadle, M.J., John, B.E., Schwartz, J.J., 2008. The rate of oceanic detachment faulting at Atlantis Bank, SW Indian Ridge. *Earth Planet. Sci. Lett.* 273, 105–114.
- Bernasconi, S.M., et al., 2021. InterCarb: a community effort to improve interlaboratory standardization of the carbonate clumped isotope thermometer using carbonate standards. *Geochem. Geophys. Geosyst.* 22 (5).
- Booij, E., Gallahan, W.E., Staudigel, H., 1995. Ion-exchange experiments and Rb/Sr dating on celadonites from the Troodos ophiolite, Cyprus. *Chem. Geol.* 126, 155–167.
- Cheng, H., Edwards, R.L., Hoff, J., Gallup, C.D., Richards, D.A., Asmerom, Y., 2000. The half-lives of uranium-234 and thorium-230. *Chem. Geol.* 169, 17–33.
- Clark, T.R., Zhao, J.X., Roff, G., Feng, Y.-X., Done, T.J., Nothdurft, L.D., Pandolfi, J.M., 2014. Discerning the timing and cause of historical mortality events in modern Porites from the Great Barrier Reef. *Geochim. Cosmochim. Acta* 138, 57–80.
- Coggon, R.M., Teagle, D.A.H., Smith-Duque, C.E., Alt, J.C., Cooper, M.J., 2010. Reconstructing past seawater Mg/Ca and Sr/Ca from mid-ocean ridge flank calcium carbonate veins. *Science* 327 (5969), 1114–1117.
- Coogan, L.A., Parrish, R.R., Roberts, N.M.W., 2016. Early hydrothermal carbon uptake by the upper oceanic crust: Insight from in situ U-Pb dating. *Geology* 44, 147–150.
- Daëron, M., Blamart, D., Peral, M., Affek, H.P., 2016. Absolute isotopic abundance ratios and the accuracy of $\Delta 47$ measurements. *Chem. Geol.* 442, 83–96.
- Daëron, M., Drysdale, R.N., Peral, M., Huyghe, D., Blamart, D., Coplen, T.B., Lartaud, F., Zanchetta, G., 2019. Most Earth-surface calcites precipitate out of isotopic equilibrium. *Nat. Commun.* 10, 429. <https://doi.org/10.1038/s41467-019-08336-5>.
- Dick, H.J.B., MacLeod, C.J., Blum, P., Abe, N., Blackman, D.K., Bowles, J.A., Cheadle, M.J., Cho, K., Cizuela, J., Deans, J.R., Edgcomb, V.P., Ferrando, C., France, L., Ghosh, B., Iddefonse, B., John, B., Kendrick, M.A., Koepke, J., Leong, J.A.M., Liu, C., Ma, Q., Morishita, T., Morris, A., Natland, J.H., Nozaka, T., Pluempner, O., Sanfilippo, A., Sylvan, J.B., Tivey, M.A., Tribuzio, R., Viegas, G., 2019. Dynamic accretion beneath a slow-spreading ridge segment: IODP Hole 1473A and the Atlantis Bank oceanic core complex. *J. Geophys. Res., Solid Earth* 124, 12631–12659. <https://doi.org/10.1029/2018JB016858>.
- Dick, H.J.B., Natland, J.H., Alt, J.C., Bach, W., Bideau, D., Gee, J.S., Haggas, S., Hertogen, J.G.H., Hirth, G., Holm, P.M., Iddefonse, B., Iturrino, G.J., John, B.E., Kelley, D.S., Kikawa, E., Kingdon, A., LeRoux, P.J., Maeda, J., Meyer, P.S., Miller, D.J., Naslund, H.R., Niu, Y.-L., Robinson, P.T., Snow, J.E., Stephen, R.A., Trimby, P.W., Worm, H.-U., Yoshinobu, A., 2000. A long in situ section of the lower oceanic crust: results of ODP Leg 176 drilling at the Southwest Indian Ridge. *Earth Planet. Sci. Lett.* 179, 31–51.
- Eickmann, B., Bach, W., Rosner, M., Peckmann, J., 2009. Geochemical constraints on the modes of carbonate precipitation in peridotites from the Logatchev Hydrothermal Vent Field and Gakkel Ridge. *Chem. Geol.* 268 (1), 97–106.
- Eiler, J.M., 2007. "Clumped-isotope" geochemistry - the study of naturally-occurring, multiply-substituted isotopologues. *Earth Planet. Sci. Lett.* 262 (3–4), 309–327.
- Fowler, A.P.G., Zierenberg, R.A., Reed, M.H., Palandri, J., Óskarsson, F., Gunnarsson, I., 2019. Rare earth element systematics in boiled fluids from basalt-hosted geothermal systems. *Geochim. Cosmochim. Acta* 244, 129–154.
- Gillis, K.M., et al., 2014. Geochemistry summary. In: Gillis, K.M., Snow, J.E., Klaus, A., Scientists, E. (Eds.), *Proceedings of the Integrated Ocean Drilling Program*, vol. 345. Integrated Ocean Drilling Program, College Station, TX, pp. 1–7.
- Hart, S.R., Blusztajn, J., Dick, H.J.B., Meyer, P.S., Muehlenbachs, K., 1999. The fingerprint of seawater circulation in a 500-meter section of ocean crust gabbros. *Geochim. Cosmochim. Acta* 63, 4059–4080.
- Hemingway, J.D., Henkes, G.A., 2021. A disordered kinetic model for clumped isotope bond reordering in carbonates. *Earth Planet. Sci. Lett.* 566, 116962.
- John, B.E., Foster, D.A., Murphy, J.M., Cheadle, M.J., Baines, A.G., Fanning, C.M., Copeland, P., 2004. Determining the cooling history of in situ lower oceanic crust—Atlantis Bank, SW Indian Ridge. *Earth Planet. Sci. Lett.* 222, 145–160.
- Kendrick, M.A., 2019. Halogens in Atlantis Bank gabbros, SW Indian Ridge: implications for styles of seafloor alteration. *Earth Planet. Sci. Lett.* 514, 96–107.
- Kendrick, M.A., Caulfield, J., Nguyen, A., Zhao, J.-X., Blakey, I., 2020a. Halogen and trace element analysis of carbonate-veins and Fe-oxyhydroxide by LA-ICPMS: implications for seafloor alteration on the Atlantis Bank, SW Indian Ridge. *Chem. Geol.* 547, 119668.
- Kendrick, M.A., Danyushevsky, L., Falloon, T., Woodhead, J.D., Arculus, R., Ireland, T., 2020b. SW Pacific arc and backarc lavas and the role of slab-bend serpentinites in the global halogen cycle. *Earth Planet. Sci. Lett.* 530, 115921.
- Kim, S.T., Mucci, A., Taylor, B.E., 2007. Phosphoric acid fractionation factors for calcite and aragonite between 25 and 75 °C: revisited. *Chem. Geol.* 246, 135–146.
- Kim, S.T., O'Neil, J.R., 1997. Equilibrium and nonequilibrium oxygen isotope effects in synthetic carbonates. *Geochim. Cosmochim. Acta* 61, 3461–3475.
- Laureijs, C.T., Coogan, L.A., Spence, J., 2021. In-situ Rb-Sr dating of celadonite from altered upper oceanic crust using laser ablation ICP-MS/MS. *Chem. Geol.* 579. <https://doi.org/10.1016/j.chemgeo.2021.120339>.
- Lloyd, Max, 2020. ClumpyCool. OSF, April 23. <https://doi.org/10.17605/OSF.IO/JYHSW>.
- Ludwig, K.R., 2012. User's Manual for Isoplot 3.7. Berkeley Geochronology Center Special Publication, vol. 4.
- MacDonald, J.M., Faithfull, J.W., Roberts, N.M.W., Davies, A.J., Holdsworth, C.M., Newton, M., Williamson, S., Boyce, A., John, C.M., 2019. Clumped-isotope paleothermometry and LA-ICP-MS U-Pb dating of lava-pile hydrothermal calcite veins. *Contrib. Mineral. Petrol.* 174.
- MacLeod, C., Dick, H.J.B., Blum, P., Abe, N., Blackman, D.K., Bowles, J.A., Cheadle, M.J., Cho, K., Cizuela, J., Deans, J.R., Edgcomb, V.P., Ferrando, C., France, L., Ghosh, B., Iddefonse, B., Kendrick, M.A., Koepke, J.H., Leong, J.A.M., Liu, C., Ma, Q., Morishita, T., Morris, A., Natland, J.H., Nozaka, T., Pluempner, O., Sanfilippo, A., Sylvan, J.B., Tivey, M.A., Tribuzio, R., Viegas, L.G.F., 2017. Southwest Indian Ridge Lower

- Crust and Moho. In: *Proceedings of the International Ocean Discovery Program*, vol. 360. College Station, TX.
- McArthur, J.M., Howarth, R.J., Bailey, T.R., 2001. Strontium isotope stratigraphy: LOWESS Version 3. Best fit line to the marine Sr-isotope curve for 0 to 509 Ma and accompanying look-up table for deriving numerical age. *J. Geol.* 109, 155–169.
- Meckler, A.N., Ziegler, M., Millan, M.L., Breitenbach, S.F.M., Bernasconi, S.M., 2014. Long-term performance of the Kiel carbonate device with a new correction scheme for clumped isotope measurements. *Rapid Commun. Mass Spectrom.* 28 (15), 1705–1715.
- Natland, J.H., Dick, H.J.B., Miller, D.J., Von Herzen, R.P. (Eds.), 2002. *Returning to Hole 735B. Proceedings ODP Scientific Results Leg 176. College Station TX (Ocean Drilling Program).*
- Nozaka, T., Akitou, T., Abe, N., Tribuzio, R., 2019. Biotite in olivine gabbros from Atlantis Bank: evidence for amphibolite-facies metasomatic alteration of the lower oceanic crust. *Lithos* 348.
- Paton, C., Hellstrom, J., Paul, B., Woodhead, J., Hergt, J., 2011. Lolite: freeware for the visualisation and processing of mass spectrometric data. *J. Anal. At. Spectrom.* 26, 2508–2518.
- Pourmand, A., Dauphas, N., Ireland, T.J., 2012. A novel extraction chromatography and MC-ICP-MS technique for rapid analysis of REE, Sc and Y: revisiting CI-chondrite and Post-Archean Australian Shale (PAAS) abundances. *Chem. Geol.* 291, 38–54.
- Rioux, M., Cheadle, M.J., John, B.E., Bowring, S.A., 2016. The temporal and spatial distribution of magmatism during lower crustal accretion at an ultraslow-spreading ridge: high-precision U–Pb zircon dating of ODP Holes 735B and 1105A, Atlantis Bank, Southwest Indian Ridge. *Earth Planet. Sci. Lett.* 449, 395–406.
- Roberts, N.M.W., Rasbury, E.T., Parrish, R.R., Smith, C.J., Horstwood, M.S.A., Condon, D.J., 2017. A calcite reference material for LA-ICP-MS U–Pb geochronology 18 (7), 2807–2814.
- Schroeder, T., Bach, W., Jons, N., Jons, S., Monien, P., Klugel, A., 2015. Fluid circulation and carbonate vein precipitation in the footwall of an oceanic core complex, Ocean Drilling Program Site 175, Mid-Atlantic Ridge. *Geochem. Geophys. Geosyst.* 16 (10), 3716–3732.
- Schwartz, J.J., John, B.E., Cheadle, M.J., Reiners, P.W., Baines, A.G., 2009. Cooling history of Atlantis Bank oceanic core complex: evidence for hydrothermal activity 2.6 Ma off axis. *Geochem. Geophys. Geosyst.* 10.
- Staudacher, T., Allègre, C.J., 1988. Recycling of oceanic crust and sediments: the noble gas subduction barrier. *Earth Planet. Sci. Lett.* 89, 173–183.
- Staudigel, H., 2014. 4.16 - Chemical fluxes from hydrothermal alteration of the oceanic crust. In: Holland, H., Turekian, K.K. (Eds.), *Treatise of Geochemistry*, 2nd edition, pp. 583–606.
- Staudigel, H., Hart, S.R., 1985. Dating of ocean crust hydrothermal alteration: strontium isotope ratios from Hole 504B carbonates and the re-interpretation of Sr isotope data from Deep Sea Drilling Project Sites 105, 332, 417, and 418. In: Anderson, R.N., Honnorez, J., Becker, K. (Eds.), *Initial Reports DSDP. Govt. Printing Office*, pp. 297–303.
- Stein, C.A., Stein, S., 1992. A model for the global variation in oceanic depth and heat-flow with lithospheric age. *Nature* 359, 123–129.
- Stolper, D.A., Eiler, J.M., 2015. The kinetics of solid-state isotope-exchange reactions for clumped isotopes: a study of inorganic calcites and apatites from natural and experimental samples. *Am. J. Sci.* 315, 363–411.
- Ternieten, L., Früh-Green, Bernasconi, S.M., 2021. Distribution and sources of carbon in serpentinized mantle peridotites at the Atlantis Massif (IODP Expedition 357). *J. Geophys. Res., Solid Earth* 126 (10).
- Vanko, D.A., Stakes, D., 1991. 9. Fluids in oceanic layer 3: evidence from veined rocks, Hole 735B, Southwest Indian Ridge. *Proc. Ocean Drill. Program Sci. Results* 118, 183–215.